Department of Veterans Affairs

Journal of Rehabilitation Research and Development Vol 32 No. 3, October 1995
Pages 245–254

Strain-based fatigue analysis of wheelchairs on a double roller fatigue machine

J. David Baldwin, PhD and John G. Thacker, PhD
School of Aerospace and Mechanical Engineering, University of Oklahoma, Norman, OK 73019; Department of Mechanical, Aerospace, and Nuclear Engineering, University of Virginia, Charlottesville, VA 22903

Abstract—Results are presented from an experimental program that recorded the outputs of strain gages mounted on two wheelchair frames (one manual, one power) as the wheelchairs were run on a double roller fatigue machine. Rectangular strain gage rosettes were attached to the frames near the cross tube center pin and on the side frame behind a front caster. Thirty data sets were recorded from each rosette on each wheelchair frame. The fatigue test machine and test protocol were in substantial conformance with the recently published ANSI/RESNA Standard for wheelchair fatigue testing.

Two analyses have been performed on the recorded strain data. The von Mises stress histories were computed from the strain data and show that peak stresses are frequently twice the mean value. Also, estimates of the number of fatigue machine cycles to failure have been made using a strain-based fatigue analysis. These data will provide wheelchair designers with useful data to incorporate into their design process.

Key words: *double roller fatigue machine, fatigue, strain, wheelchair.*

This material is based on work supported by the National Institute on Disability and Rehabilitation Research, U.S. Department of Education.
Address all correspondence and requests for reprints to: J. D. Baldwin, PhD, School of Aerospace and Mechanical Engineering, University of Oklahoma, Norman, OK 73019.

INTRODUCTION

Any load bearing metal structure subjected to variable loads is a candidate for fatigue failure. The widely studied phenomenon of metal fatigue has long been known to be a principal failure mode of components carrying dynamic loads even though the stresses are significantly below the material's yield strength. Because failures can occur at loads lower than those considered for static failure, the designer of such dynamically loaded structures must consider sufficient fatigue life as a primary design constraint.

Metal fatigue analysis is complicated by two factors. First, fatigue failures can be thought of as the culmination of two processes: fatigue crack initiation and crack propagation to failure. In the ideal case, the designer will have full knowledge of the time-varying loads imposed on the structure and will have a fatigue theory available that can accurately predict the failure of the critical sections of the structure. In reality, the loading is not often known with complete accuracy and our crack initiation models are simplified curve fits based on experimental observations. Similarly, crack propagation models, such as the Paris relation

$$\frac{da}{dN} = C\,(\Delta K)^n$$

are also based on empirical formulations. In Equation 1, a is the crack length, N is the number of

Journal of Rehabilitation Research and Development Vol. 32 No. 3 1995

loading cycles, ΔK is the stress intensity at the crack tip and C and n are curve fit parameters for a given material.

The second issue that complicates a fatigue analysis (and one that is usually ignored) is the fact that the fatigue lives of highly polished specimens tested under nominally identical situations can fail at lives that vary by over one order of magnitude (1,2). Efforts at incorporating this fundamental, material-based, life scatter have been mainly of theoretical interest up to this point.

Given the uncertainties associated with the analysis and design of a dynamically loaded structure, the designer is often left with no alternative other than to perform fatigue tests on prototypes to assess the adequacy of the structure. In fact, the fatigue test may be imposed on the manufacturer by contract or regulatory requirements.

The purpose of this paper is to present recorded strain data taken from two wheelchairs as they were driven on a double roller fatigue machine and to illustrate a strain-based fatigue analysis that may be useful in estimating the fatigue life based on the response data. Stress histories computed from the strains are also presented. The stress versus time histories illustrated here could be useful to a wheelchair designer in the preliminary stress analysis design phase. Our data establish order of magnitude values for some stress measures used in design and show the stress variability experienced on a double roller fatigue machine. Although our machine was built before the circulation of the latest wheelchair fatigue test standard, *ANSI/RESNA WC/08: RESNA Standard: Wheelchairs - Static, Impact and Fatigue Strength Tests* (3,4), it is in substantial conformance with that standard. It should be emphasized, however, that the wheelchairs used in this investigation were not tested to failure. They were being used concurrently in other projects and could not be sacrificed for this one. As a result, the fatigue life predictions illustrated here have not been verified by actual test data.

The results reported here are strictly applicable to the two wheelchairs tested. These data will be useful, however, in guiding wheelchair designers as they prepare their structures for an ANSI/RESNA Standard fatigue test. The fatigue life analysis may also be useful in stimulating discussion among designers about the long-term survivability of their designs.

METHODS

Current Test Program

The testing program described in this paper was part of a larger effort to record dynamic strain histories from wheelchair frames as they traversed different terrains. Experimentally measured strain histories were to be used as the input data for a fatigue reliability analysis of wheelchair structural elements; the structural reliability model was to be incorporated into an integrated electro-mechanical wheelchair system reliability analysis.

Two wheelchairs were used in the testing: an Invacare Rolls IV (manual) and an Invacare Rolls Arrow (power). Both wheelchairs were of the folding type with two steel cross tubes pinned together at the center. The tube carbon steel alloy was assumed to be 1010-1020 grade commonly used in steel wheelchair frames; no metallurgical analysis was done to verify this assumption. The manual wheelchair had solid front and rear tires and chrome plated frame tubes. Front tire dimensions on this wheelchair were 20 cm (7.9 in) diameter by 1.9 cm (0.75 in) radial thickness. The manual wheelchair's solid rear tires were 50.8 cm (20 in) diameter by 5.4 cm (2.125 in) radial thickness. The power wheelchair had solid front tires and pneumatic rear tires and painted frame tubes. On this chair, the front tires had an outside diameter of about 19 cm (7.5 in) and a radial thickness of about 3.8 cm (1.5 in); dimensions of the rear tires were 61.0 cm (24 in) outside diameter by 1.3 cm (0.5 in) radial thickness. Seventy pounds of steel plates were substituted for batteries on the power chair.

As described below, strain gages were attached to the wheelchair frames and connected to a data acquisition system. The strain gage installations were identical on both wheelchair frames. Test results and analysis of the stress histories for the wheelchairs rolling over bumps on a treadmill and falling off an elevated platform were reported previously (5).

Instrumentation

Three rectangular strain gage rosettes were attached in approximately the same locations to each wheelchair frame. Two rosettes were located on the front cross tube, one directly below the center connecting bolt on the bottom of the tube, and the other on the front of the tube next to the bolt. These

gages were designated "XG1" and "XG2." The third rosette was mounted on the horizontal tube directly behind the right front caster and was designated "CG1" (**Figure 1**). The cross tube gage locations were chosen because this area of the frame has been shown to be subjected to high stresses under static loading (6). The caster location was chosen to measure the tube response to front caster impacts, such as those experienced on the double-roller fatigue machine. Each strain sensing element of the rosette was connected to a Wheatstone bridge in a quarter bridge pattern. The bridge output voltage was amplified by a strain gage conditioner, filtered by a low pass filter and sampled by a computer-mounted data acquisition board. The assumption has been made that each strain gage element is in a field of essentially uniform strain (i.e., small strain gradients) and that the strains at nearby geometric discontinuities can be computed, by an appropriate strain concentration factor, from the recorded strains. The strain gage installations and data acquisition system used in this study were the same as those reported in Baldwin and Thacker (5), to which the reader is referred for details.

Test Regime

The wheelchairs were tested on the double roller fatigue machine developed in 1986 at the University of Virginia (4). Any variances from the ANSI/RESNA test standard procedure (3), the "test standard," will be noted.

The double roller fatigue machine consisted of two 91.4 cm (36 in) long by 27.3 cm (10.75 in) diameter aluminum rollers mounted on a steel channel frame. Each roller had two rectangular slats, 30.5 cm (12 in) long by 1.3 cm (0.5 in) high by 3.8 cm (1.5 in) wide attached to the surface. On either roller, the slats were oriented 180° apart (i.e., the slat on the left end of the roller was located 180° around the circumference of the roller from the slat on the right end). The slats provided "texture" to the rolling surface. The rollers were positioned so that no two tires were in contact with their respective slat simultaneously during the rotation. These dimensions are within the ranges given in the test standard.

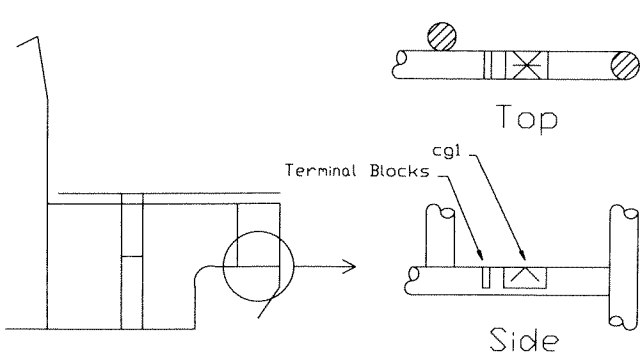

Figure 1.
Rosette CG1 installation site.

A 560 W (¾ HP) electric motor drove the back roller through a right angle gear head; a toothed belt running over pulleys transmitted torque from the back roller to the front roller. The motor turned the back roller at approximately 60 revolutions per minute (RPM) which translates into a roller surface speed of approximately 0.86 m/s. The test standard specifies a surface speed of 1.0 ± 0.1 m/s.

For this investigation, the pulleys were the same diameter; thus, the front roller turned at the same RPM as the rear. The test standard specifies that the speed of the roller under the wheels that are not being driven (in this case, the front wheels) are 2–7 percent faster than the other drum. The front roller was mounted so that the roller's axis made an angle of 5° with its axis of rotation; the front axis of rotation was horizontal and parallel with the rear roller's axis. Making the axes offset caused a reversed torque to be applied to the frame through the front casters on each revolution. The test standard specifies that the roller axes are horizontal. The difference in the test data due to these two variances from the test standard is not known. It is felt, however, that the cyclic loading on the frame caused by off-axis rollers is more severe than that due to a speed differential between the rollers and that the test data reported here reflects a harsher test than the test standard.

Surrounding the fatigue machine bed frame was a set of support bars that attached to the rear axles of the wheelchair under test to maintain these wheels in the correct position with respect to the rear roller. Note that the rear wheels were only restrained from side to side (i.e., along the axis of the roller) and from front to back. The wheelchair was free to move vertically. The front casters were free to bounce.

Once the wheelchair was positioned on the rollers and its rear axles attached to the support bars, one of its strain gages was connected into the instrumentation system. The test protocol specified

Journal of Rehabilitation Research and Development Vol. 32 No. 3 1995

that any strain gage under test was to have been continuously energized for 24 hours before the beginning of the test. This period was sufficient for the gages to warm up and for any thermal transients to die out. With the wheelchair unloaded and resting on a temporary flat platform above the rollers, the strain gage circuit was balanced to show zero strain output. The platform was removed, the wheelchair was lowered onto the rollers, and the chair was then loaded with 100 kg of weight in the seat and 10 kg on the footrests. The ISO standard 100 kg load dummy (4,7) was secured with straps to the wheelchair seat and back. The dummy was loosely tethered from an overhead gantry that would support the weight in case of failure of the wheelchair frame.

Strain Data Preparation

A data collection run consisted of recording the output of one strain gage rosette for 4 sec as the wheelchair was run on the double roller fatigue machine. The data was sampled at a rate of 512 samples/sec/gage element; thus, the strain signal consisted of 2048 data points recorded from each of the three rosette arms. The analog voltage data was digitized and stored on disk in terms of integers in the interval −2047 through +2048. The quantity of data that could be recorded in a test was limited by the memory capacity of the data acquisition computer. Four sec of data corresponded to approximately four complete revolutions of the fatigue machine rollers.

The first step in preparing the digital strain data was to convert them back into engineering strain values. In this calculation, the strain gage outputs were corrected for gage transverse sensitivity and nonlinearity. Then, using the strain transformation rule, the three elements of rosette strain could be expressed as the strain existing at any specified angle from the rosette. Specifically, if the strains recorded from rosette arms 1, 2, and 3 are labeled ϵ_0, ϵ_{45}, and ϵ_{90}, respectively, the strain existing at any angle ϕ is given by

$$\epsilon_\phi = \frac{\epsilon_0 + \epsilon_{90}}{2} + \frac{\epsilon_0 - \epsilon_{90}}{2} \cos 2\phi + \frac{2\epsilon_{45} - (\epsilon_0 + \epsilon_{90})}{2} \sin 2\phi \qquad [2]$$

For the data presented and discussed here, the strains at 45° from rosette arm 1 were used in the fatigue analysis. These strains were collinear with rosette arm 2 that was always aligned along the axis of the frame tube; in this case, Equation 2 reduces to $\epsilon_\phi = g_{45}$. In principle, however, the strains at any angle could have been used.

Beyond using the strain gage outputs in fatigue calculations, we also used them to compute the von Mises stress histories at the gage locations. The von Mises stress can be calculated from rectangular strain gage rosette outputs by first computing the principal normal strains. At any sampling instant, the principal normal strains, ϵ_1 and ϵ_2, can be expressed in terms of the instantaneous rosette arm output strains using the relationship

$$\epsilon_{1,2} = \frac{\epsilon_0 + \epsilon_{90}}{2} \pm \frac{\sqrt{(\epsilon_0 - \epsilon_{90})^2 + [2\epsilon_{45} - (\epsilon_0 + \epsilon_{90})]^2}}{2} \qquad [3]$$

and the instantaneous principal stresses, σ_1 and σ_2, are given by,

$$\sigma_1 = \frac{E}{1-\nu^2}(\epsilon_1 + \nu\epsilon_2)$$
$$\sigma_2 = \frac{E}{1-\nu^2}(\epsilon_2 + \nu\epsilon_1) \qquad [4]$$

where ν is the tube material Poisson ratio. In terms of the principal stresses, the instantaneous von Mises stress is given by

$$\sigma_e = \sqrt{\sigma_1^2 + \sigma_2^2 - \sigma_1\sigma_2} \qquad [5]$$

Fatigue Life Model

Using the histories recorded from the strain gages, an estimate was made of the fatigue life of each gage location. The life estimate was made using a strain-based fatigue analysis. The primary assumption involved in the strain-based fatigue model is that the appearance of a crack in a component can be related to the fracture of a small specimen in a fatigue test. This method has been shown (8) to be reasonably accurate in predicting cracking in test specimens subjected to complex load histories. The strain-based analysis carried out in this investigation was explained in more detail in references 9–11.

When a metal specimen is loaded such that the possibility of plastic deformation exists, we must use a constitutive relationship that reflects this fact.

Even moderate stresses can be magnified by the presence of a geometric discontinuity (stress concentration) to the point where localized plasticity occurs. The linear elastic stress-strain relationship, $\sigma = E\epsilon$, is inadequate in the situation where plastic strains are present. In contrast to a monotonic stress-strain relationship, a cyclic stress-strain expression is necessary when examining the inelastic response due to fatigue loading.

The cyclic stress-strain curve is given by Landgraf, et al. (12)

$$\epsilon = \frac{\sigma}{E} + \left(\frac{\sigma}{K'}\right)^{\frac{1}{n'}} \qquad [6]$$

The first and second terms of Equation 6 represent the elastic and plastic contributions to the total strain, respectively. The parameters K' and n', called the cyclic strain hardening coefficient and the cyclic strain hardening exponent, respectively, are material properties derived from laboratory tests. In the strain-based fatigue method, Equation 6 is used to model the material response to the first load application.

After the first load application, especially if there is inelastic strain, the material will exhibit hysteresis. This means that upon unloading the stress-strain does not follow the loading curve. We model the behavior of the material as it follows the *hysteresis stress-strain curve,* which is given by

$$\Delta\epsilon = \frac{\Delta\sigma}{E} + 2\left(\frac{\Delta\sigma}{2K'}\right)^{\frac{1}{n'}} \qquad [7]$$

Equations 6 and 7 represent the fundamental material response (stress-strain) to cyclic loading.

While the average strain in the smooth areas of a structural member can be measured with a strain gage, the strain near a notch or other discontinuity is not so easily measured. Neuber (13) found that for an edge notch geometry, the theoretical stress concentration factor, K_t, is related to the stress concentration factor, K_σ, and the strain concentration factor, K_ϵ by the equation

$$K_t^2 = K_\sigma K_\epsilon \qquad [8]$$

The nominal stress s and the nominal strain e are measured outside the notch strain gradient. If the measured (remote) strain remains elastic, that is, $s = Ee$, *Neuber's rule becomes*

$$\sigma\,\epsilon = (K_t\, e)^2\, E \qquad [9]$$

Note that Equation 9 is valid only for the first load cycle, where the σ–ϵ curve is the constitutive relation. In a manner similar to the cyclic stress-strain curve, Neuber's rule is modified to handle all strain reversals after the first. The "hysteresis Neuber's rule" corresponding to the hysteresis stress-strain curve is

$$\Delta\sigma\,\Delta\epsilon = (K_t\,\Delta e)^2\, E \qquad [10]$$

The (possibly inelastic) strains and stresses appearing in Equations 9 and 10 are related through the cyclic stress-strain and hysteresis stress-strain constitutive relationships (Equations 6 and 7). Because the cyclic stress-strain equations and Neuber's rule provide unique relationships between stress and strain, the two equations must be solved simultaneously at each strain reversal. This is called a *notch strain analysis.* Of course, if a more accurate finite element or experimentally determined notch strain calibration is available, it should be used for the Neuber analysis. Globally convergent iterative solutions for the Neuber notch strain analysis can be obtained using Newton's method (9).

Using the cyclic stress strain curves, (Equations 6 and 7), and Neuber's model for the notch strains in way of a geometric discontinuity, (Equations 9 and 10), we can convert a strain history recorded away from the stress riser to a strain history at the root of the notch. For a highly variable history, the strain cycles (which will be used to estimate the number of cycles to failure) are not readily apparent. In such a case, we choose a technique known as "rainflow cycle counting" (14) to identify the closed stress-strain loops from the history. The rainflow cycle counting procedure given by Downing and Socie (15) has been implemented to convert the computed notch strain history to a series of constant amplitude strain cycles for comparison with the strain-life curve.

The elastic-plastic strain life (ϵ–N) relationship, given by

$$\frac{\Delta\epsilon}{2} = \frac{\sigma_f'}{E}(2N_f)^b + \epsilon_f'(2N_f)^c \qquad [11]$$

has been used to model the failure of smooth laboratory specimens subjected to cyclic elastic and plastic strain. In Equation 11, the quantity $2N_f$ is the number of strain cycles to failure at strain range $\Delta\epsilon$;

Journal of Rehabilitation Research and Development Vol. 32 No. 3 1995

parameters E, σ_f', b, ϵ_f', and c are the modulus of elasticity, fatigue strength coefficient, fatigue strength exponent, fatigue ductility coefficient and fatigue ductility exponent, respectively. The strain range $\Delta\epsilon$ is that for each closed stress-strain hysteresis loop identified by the rainflow cycle counting procedure. The number of strain cycles to failure at a given strain range can be computed iteratively from Equation 11 using Newton's method. This iteration can also be shown to be globally convergent.

Equation 11 implies that for arbitrarily small strain ranges, the number of cycles to failure can become very large. Because computers cannot represent arbitrarily large and small numbers without loss of precision, some limit is placed on how large a value of N_f can be accurately computed. Also, large values of N_f begin to lose their significance when it is realized that such a large number of cycles could not be realized in a device's anticipated life. For these reasons, if a given strain range resulted in $N_f \geq 10^{10}$ cycles in Equation 11, the reported number of cycles to failure was set to 10^{10}. In practice, this upper limit could be set to any value deemed reasonable.

Miner's linear cumulative damage rule

$$D = \sum_i D_i = \sum_i \frac{n_i(\Delta\epsilon)}{N_f(\Delta\epsilon)} \qquad [12]$$

is used to compute the damage D for a block of strain loading. In Miner's rule, $n_i(\Delta\epsilon)$ is the number of strain cycles of range $\Delta\epsilon$ as found by the rainflow cycle counting procedure, $N_f(\Delta\epsilon)$ is the number of strain cycles to failure at range $\Delta\epsilon$ as given by the strain-life curve, Equation 11, and the index i runs over the collection of strain cycles. Failure is assumed to occur when the damage sum is equal to 1.0. In the strain-based analysis, failure is assumed to occur at the appearance of a small crack, typically 2.5 mm, or 0.1 in (8). If the damage sum for a given strain history is less than 1.0, failure is predicted after the occurrence of more than one block of that history. In such a case, the number of blocks to failure is given by

$$blocks = \frac{1.0}{\sum_i D_i} \qquad [13]$$

For purposes of fatigue analysis, the wheelchair frames were assumed to be made of cold-drawn 1010 carbon steel, or equivalent. The relevant fatigue properties were as listed below (16):

σ_f'	= 538 MPa (78,000 psi)	b	= −0.073
ϵ_f'	= 0.110	c	= −0.410
K'	= 490 MPa (71,000 psi)	n'	= 0.110
E	= 200 GPa (29,000,000 psi)	ν	= 0.30

RESULTS

Each wheelchair was tested on the fatigue machine while each of its three strain gages was monitored in turn. A test series consisted of recording the output of one strain gage for a total of 30 intervals of 4 sec each. Therefore, there was a total of 180 strain records; each was 4 sec long and consisted of the output of the three arms of a single strain gage rosette. We believe this data set represents the most comprehensive ever recorded from a double roller fatigue machine.

Because it would be impractical to present full details of these data sets here, two key aspects of the data will be examined. First, the nature of the von Mises stresses for the six strain gage installations will be illustrated. The von Mises stress is a commonly used measure of the potential for inelastic deformation in steels. These data will be presented in condensed form by showing von Mises stress versus time histories form one selected data set from each test series. Second, the computed number of 4-sec blocks to failure will be summarized for each test series. The failure estimates were computed using the strain-based fatigue analysis.

Recorded Stress Peaks

For each of the six test series, the von Mises stress history of one of the data sets will be discussed. Specifically, the last data set of the test series will be used in this illustration. The last data set was chosen because, by the time it was recorded, the wheelchair had stabilized on the fatigue machine and was running smoothly. For each chosen data set, the von Mises stress at each time increment was calculated using Equations 2–5; the maximum, mean, and minimum values are given in **Table 1.** Note that no stress concentration factors were incorporated into the stress computations; the stresses are as measured at the strain gages, not near geometric discontinuities. The "Data Set Number"

column contains the data set index number ("DRF xxx") and the wheelchair and rosette under test ("y-zzz").

Computed Lives and Statistical Analysis

Each of the 180 strain gage rosette data sets was analyzed using the fatigue life estimating procedures outlined above. The estimated number of 4-sec strain blocks to failure for each data set was computed using the strain life curve (Equation 11). **Table 2** summarizes the maximum, mean, minimum, and the standard deviation of the number of blocks to failure for each data set. The stress concentrations factors, K_t, used in the notch strain calculations were computed from empirical correlations given in reference 17 (K_t = 4.77 for rosette XG1) and reference 18 (K_t = 2.94 for rosette CG1). Because an earlier analysis (5) showed that the cross tube loading was predominantly bending and axial compression with very little cyclic torsion, the bending stress concentration factor has been used for XG1. Because it was not installed in way of a geometric discontinuity, the rosette XG2 strains had a stress concentration value of K_t = 1.0 (i.e., no stress increase).

It is important to note here that the value of the stress concentration factor for the cross tube center pin holes used here is based on a plain hole through the tube (17). In reality, these connections have smaller tubes inserted into the transverse holes that provide stiffening and reinforcement to the holes. The added reinforcement would be reflected in a value of K_t less than the value used here. At this time, there are no published values for the stress concentration factor for a tube with a stiffened transverse hole.

DISCUSSION

The von Mises stress histories for the six sample data sets are illustrated in **Figures 2–4**. The stress histories clearly show the periodic nature of the fatigue machine loading. Whereas the XG1 and XG2 responses show distinct differences between the manual and power wheelchairs, the CG1 data for the two chairs are essentially identical. **Figures 2–4** and **Table 1** show that the largest maximum and mean stresses and the largest stress ranges (maximum-minimum) occurred in the cross tubes of both wheelchairs. The stress levels and ranges behind the

Table 1.
Summary of von Mises stresses.

Data Set Number	Maximum, MPa (psi)	Mean, MPa (psi)	Minimum, MPa (psi)
DRF 180 (M-CG1)	72.1 (10,451)	19.3 (2795)	2.4 (348)
DRF 90 (P-CG1)	79.9 (11,585)	17.2 (2491)	1.0 (148)
DRF 120 (M-XG1)	116.3 (16,869)	43.5 (6311)	6.4 (935)
DRF 30 (P-XG1)	157.9 (22,904)	89.6 (12,989)	0.7 (102)
DRF 240 (M-XG2)	270.4 (39,219)	193.7 (28,092)	126.7 (18,373)
DRF 210 (P-XG2)	259.5 (37,643)	138.0 (20,018)	16.8 (2432)

Table 2.
Summary of computed blocks to failure.

Test Series	Maximum	Mean	Minimum	Standard Dev.
M-CG1 (N=30)	10,000,000,000	7,002,437,799	1,381,758,002	2,879,933,312
P-CG1 (N=30)	640,921,000	177,755,227	9,367,898	174,946,994
M-XG1 (N=30)	47,414	29,395	22,674	5921
P-XG1 (N=30)	652	254	140	117
M-XG2 (N=30)	10,000,000,000	8,711,326,648	293,108,482	3,341,680,157
P-XG2 (N=30)	10,000,000,000	10,000,000,000	10,000,000,000	0

One block = 4 seconds.

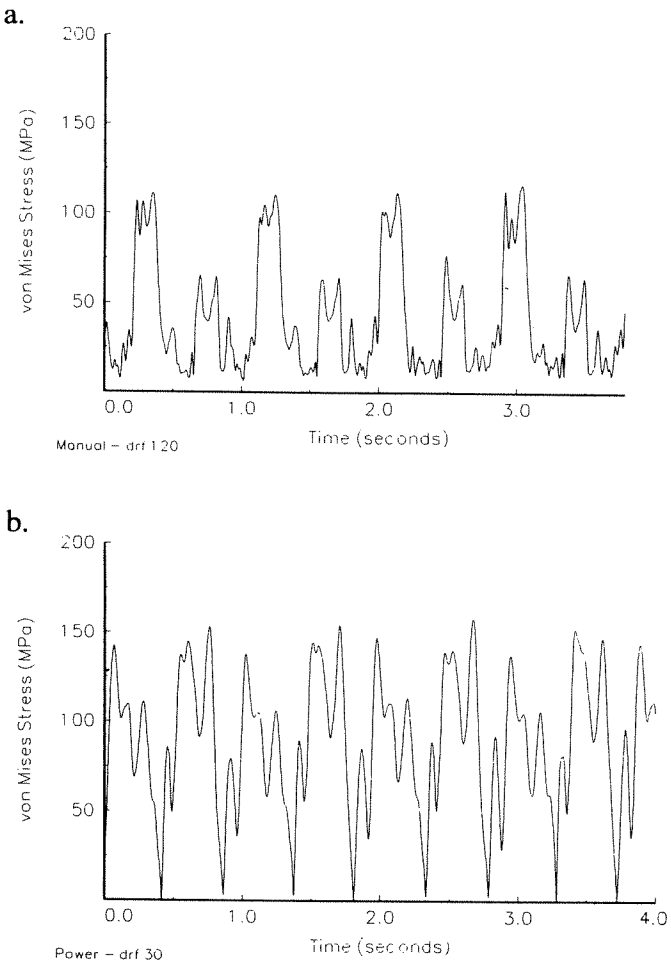

Figure 2.
von Mises stress histories for rosette XG1.

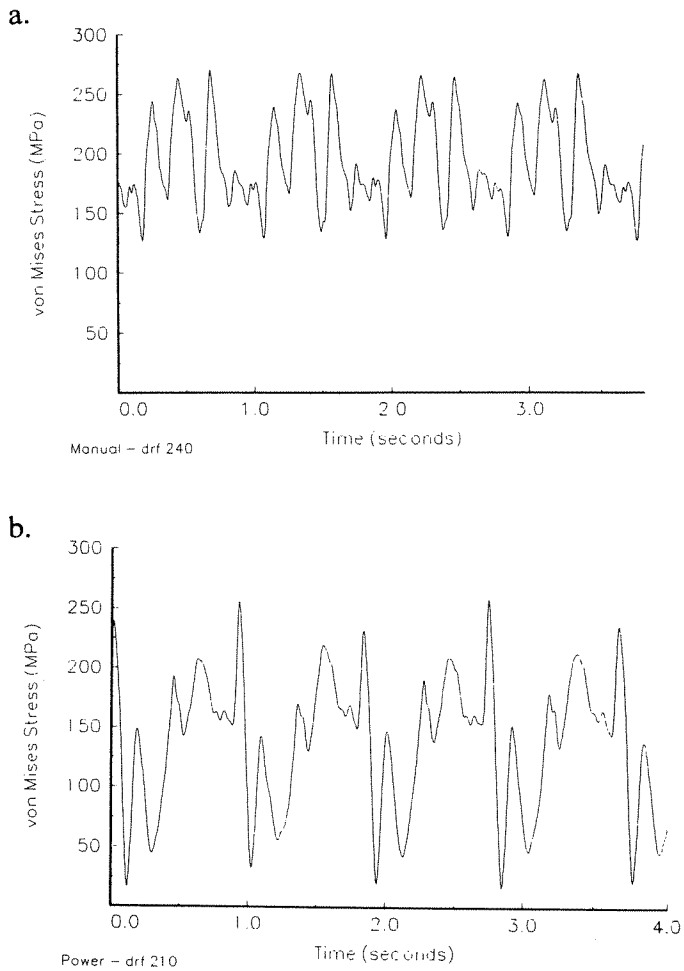

Figure 3.
von Mises stress histories for rosette XG2.

front casters were the lowest of those measured. It can also be seen that, for all three rosette locations, the power wheelchair experienced larger stress ranges than the manual wheelchair. Presumably, this result is due to the added loading on the power chair due to the batteries and drive apparatus.

It is interesting to note, however, that the maximum stresses recorded in the power wheelchair are not a great deal higher than in the manual wheelchair (and in the case of rosette XG2, are actually lower). It is felt that the comparable maximum stress levels can be attributed to the fact that, even though the tubes in the two chairs had the same outside diameter and wall thickness, the power wheelchair was slightly smaller than the manual chair, making it stiffer. The power chair's stiffer structure was able to carry its added load by developing relatively low stresses.

Table 2 summarizes the number of blocks to failure computed by the fatigue model described above. Recall that each block referred to in **Table 2** is a 4-sec history; therefore, the estimated total time to failure (in seconds) is four times the numbers given in the table. A standard wheelchair fatigue test at the University of Virginia requires a chair to survive for 100,000 cycles (roller revolutions) on the fatigue machine. This test duration corresponds to 25,000 4-sec blocks in the data presented here. It can be seen from **Table 2** that the estimated mean life for the manual wheelchair rosette XG1 is about 100,000 cycles and that the estimated mean life for the same rosette on the power wheelchair is roughly 1,000 cycles. It is felt that the low life estimates for the power wheelchair reflect the uncertainty in the value of the stress concentration factor for the cross tube center hole. If we assume that this chair is

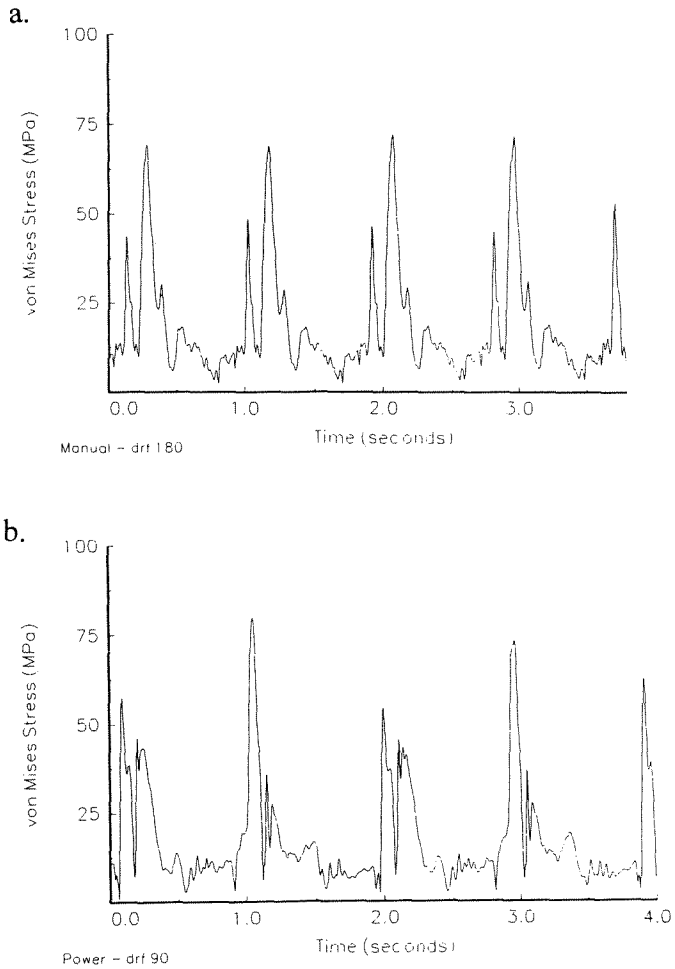

Figure 4.
von Mises stress histories for rosette CG1.

capable of surviving 100,000 cycles on the double roller fatigue machine, K_t must have a value smaller than 4.77 used here. At this time, there is no published data for the stress concentration factor for a stiffened diametral hole in a tube. The life estimates for the other rosettes on the chairs are significantly more than 100,000 cycles.

Perhaps the most striking result to be taken from this analysis is the degree of variability in the fatigue life estimates. **Table 2** shows that the standard deviations of blocks to failure are quite large, ranging from 20 percent to 98 percent of the mean. This is surprising, because one would expect the nominally identical dynamic strain histories recorded in these tests to result in life estimates of considerably less scatter. As noted earlier, the data records were initiated after the wheelchairs had stabilized on the fatigue machine and were running smoothly. It seems that a single recorded strain history of 4 sec is not sufficient to fully capture the wheelchair dynamics; perhaps longer contiguous strain samples would lead to less scatter in the fatigue life estimates. Recall that the total sampling time was limited by computer storage.

While considering the estimated fatigue lives of the wheelchair frames, the reader should bear in mind that these chairs were not tested to failure. The lives quoted here are based on a mathematical model of fatigue and have not been verified by destructive tests; as mentioned earlier, the wheelchairs were being used concurrently in other projects and were not available for a fatigue test to destruction. One should remember that the fatigue life estimates are sensitive to the value of K_t and that the values used here are approximate. We do, however, feel that the life estimates are useful in identifying locations in the frames that may be susceptible to fatigue.

CONCLUSIONS

Using strain histories recorded from two wheelchairs on a double roller fatigue machine, the von Mises stress histories and the estimated number of strain cycles to failure for three frame locations have been presented. The stress histories showed that, of the three frame locations monitored, the most highly stressed point in both wheelchairs was on the cross tube below the crossing pin at rosette XG2. The mean stress in the manual frame was about 40 percent higher than in the power frame; the manual frame peak stress was only about 4 percent larger. At rosette XG1, the power wheelchair frame experienced higher mean (106 percent higher) and maximum (36 percent higher) stresses than the manual frame. The peak stresses at XG1 for both wheelchairs were typically about 100–150 MPa lower than at XG2. It was also shown that the stresses behind the front casters at rosette CG1 were very similar between the two wheelchairs in peak magnitude and waveform. These peak stresses were approximately 200 MPa lower than those recorded at rosette XG2. The von Mises stress data could provide wheelchair builders with additional information to use in their frame strength calculations.

In contrast to the von Mises stress results where the highest stresses were recorded at rosette XG2, the fatigue calculations predicted that failure was

most likely on the side of the cross tube at the pin hole at rosette XG1. At this location, the mean life (as computed from the 30 test data sets) for the power wheelchair was about 1,000 cycles on the fatigue machine; the mean life for the manual chair was over 100,000 cycles. It is noted that the fatigue life estimate for the XG1 location is complicated by the uncertainty in the value of the stress concentration factor at that point. The mean estimated fatigue lives for the other rosette locations suggest that both wheelchairs would survive the 100,000 cycle fatigue test. The fatigue life estimates for rosette CG1 are only for the tubular joint behind the casters. This result, however, makes no statement about the strength of the caster connections to the frame tubes. It was surprising to note that the fatigue life estimates for a given frame location showed large variability for the nominally identical test data series.

Readers interested in obtaining copies of the strain histories used here may contact the lead author.

ACKNOWLEDGMENTS

This project was carried out at the University of Virginia Rehabilitation Engineering Center in Charlottesville, VA.

REFERENCES

1. Freudenthal AM. Planning and interpretation of fatigue tests. Symposium on statistical aspects of fatigue, ASTM STP-121. Philadelphia: American Society for Testing and Materials, 1952:3–22.
2. Sinclair GM, Dolan TJ. Effect of stress amplitude on statistical variability in fatigue life on 75S-T2 aluminum alloy. In: Proceedings of the American Society of Mechanical Engineers 1953:75:867–72.
3. ANSI/RESNA WC/08 1991: RESNA standard: Wheelchairs - static, impact and fatigue strength tests.
4. Duffey TM, McLaurin CA, Thacker JG. Construction and operation of the ISO double roller fatigue tester, University of Virginia Rehabilitation Engineering Center Report Number UVAREC-107-86, 1986.
5. Baldwin JD, Thacker JG. Characterization of the dynamic stress response of manual and powered wheelchair frames. J Rehabil Res Dev 1993:30:224–32.
6. Thacker JG, Todd BA, Disher TD. Stress analysis of wheelchair frames. In: Proceedings of the 8th Annual RESNA Conference, Memphis, TN. Washington, DC: RESNA Press 1985:84–6.
7. ANSI/RESNA WC/11 1991: RESNA standard: test dummies.
8. Wetzel RM, ed. Fatigue under complex loading. Warrendale PA: Society of Automotive Engineers, 1977.
9. Baldwin JD. Dynamic structural testing and strain-based fatigue reliability analysis of wheelchair frames (Dissertation). University of Virginia, 1993.
10. Baldwin JD, Thacker JG. A strain-based fatigue reliability analysis method. J Mech Des 1995:117:(A):229-34.
11. Bannantine JA, Comer JJ, Handrock JL. Fundamentals of metal fatigue analysis. Englewood Cliffs, NJ: Prentice Hall, 1990.
12. Landgraf RW, Morrow J, Endo T. Determination of the cyclic stress-strain curve. J Mater 1969:4:176–88.
13. Neuber H. Theory of stress concentration for shear-strained prismatical bodies with arbitrary nonlinear stress-strain laws. J Appl Mech 1961:E28:544–50.
14. Dowling NE. Fatigue failure predictions for complicated stress-strain histories. J Mater 1972:7:71–87.
15. Downing SD, Socie DF. Simple rainflow counting algorithms. Int J Fatigue 1982:31–40.
16. Technical report on fatigue properties - SAE J1099. SAE Handbook. Warrendale, PA: Society of Automotive Engineers.
17. Young WC. Roark's formulas for stress and strain, 6th ed. New York: McGraw-Hill, 1989.
18. Gurney TR. Fatigue of welded structures, 2nd ed. Cambridge, UK: Cambridge University Press, 1979.